Nonlinear Analysis: Modelling and Control, Vilnius, IMI, 1998, No 3

MONTE CARLO STUDY OF MULTIBARRIER HETEROSTRUCTURE SWITCH

A. Reklaitis

Semiconductor Physics Institute, A.Go š tauto 11, 2600 Vilnius, Lithuania

G. Grigaliûnaitë

Vilnius Gediminas Technical University, Saulëtekio al.11, 2040 Vilnius, Lithuania

Abstract

A multibarrier heterostructure GaAs/AlAs current switching diode has been investigated by Monte Carlo method. The switching phenomenon is based on electron tunnelling and thermoemission from the GaAs wells to the AlAs barriers, electron drift across the thin AlAs barriers followed by a subsequent impact ionisation in the undoped GaAs layers. The calculated switching voltage is close to 100 V for the diode involving four AlAs barriers at 300 K lattice temperature. The estimated switching time is in the order of 10 ps.

The switching voltage of the most developed devices is in the order of several volts [1-7]. On the other hand, high-speed switches exhibiting high switching voltage are of great importance. In [8, 9] a high voltage switching diode composed from a multibarrier GaAs/AlAs heterostructure is proposed. In the present paper this structure, is investigated by Monte Carlo simulations. The principle of operation of the voltage-controlled switch is based on the electron tunnelling process through the heterojunction interfaces, followed by subsequent interband impact ionisation and confinement of the created electrons and holes in GaAs wells.

A schematic cross section of the proposed four-barrier AlAs/GaAs switch is depicted in Fig. 1. The structure consists of the adjacent to the cathode, heavily doped GaAs layer followed by four unit cells. Each unit cell involves an undoped AlAs barrier followed by an undoped GaAs layer, and finally, by a doped GaAs layer. The donor concentration of $5x10^{18}$ cm^{-3} for the cathode and anode contacts is accepted. It is assumed that electrons in the contacts are in thermal equilibrium with the lattice. The models of GaAs and AlAs include Γ, L and X nonparabolic valleys for the conduction band, and heavy, light and split-off nonparabolic subbands for the valence band. All

basic phonon scattering processes as well as ionised impurity scattering are taken into account for the electrons and holes. The material parameters of GaAs are assumed to be the same as the ones collected in [10]. The material parameters of AlAs are taken from [11]. Band offset between the Γ valleys of GaAs and AlAs is assumed to be 1.03 eV [12].

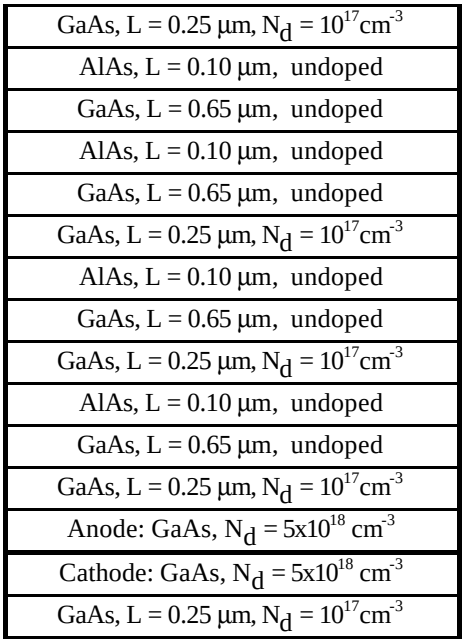

Fig. 1. A schematic cross section of the diode.

The thermionic emission and tunnelling across GaAs/AlAs heterointerfaces were considered for electrons and holes. Depending on the carrier wave vector, either a trapezoidal or a triangular potential barrier was considered for the tunnelling of each individual Monte Carlo particle impinging the barrier. The tunnelling probabilities used in the simulations were derived by using the transfer matrix approach and taking into account the discontinuity of the carrier effective mass at the heterointerfaces [8, 11].

The tunnelling probability for the trapezoidal barrier is given by Eq. (1). The three layers composing trapezoidal potential barrier are characterised by indexes 1 (layer of incident electron), 2 (barrier layer), and 3 (the final layer after the tunnelling). The obtained transmission tunnelling probability for a trapezoidal barrier is given by

$$D = \frac{4k_{3x}}{p^2 k_{1x}} \times \frac{1}{M^2}, \qquad (1)$$

where k_{1x} and k_{3x} are normal to the heterointerface wave vector components, incident and final, respectively,

$$M^2 = \Big\{ [A_i(h_0)B_i'(h_d) - A_i'(h_d)B_i(h_0)] + \frac{k_{3x}}{k_{1x}}[A_i(h_d)B_i'(h_0) - A_i'(h_0)B_i(h_d)] \Big\}^2 + \Big\{ \frac{m_1 k_F}{m_2 k_{1x}}[A_i'(h_0)B_i'(h_0) - A_i'(h_d)B_i'(h_0)] + \frac{m_2 k_{3x}}{m_1 k_F}[A_i(h_0)B_i(h_d) - A_i(h_d)B_i(h_0)] \Big\}^2$$

A_i and B_i are Airy functions, A_i' and B_i' are their derivatives, and

$$k_{3x}^2 = \frac{2m_1}{\hbar^2}(E_1 + eFd) - k_{//},$$

$$k_F = (2m_2 eF/\hbar^2)^{1/3},$$

$$h_0 = k_F(U_0 - E_{2x})/eF \quad ,$$

$$h_d = k_F(U_0 - E_{2x} - eFd)/eFd \quad ,$$

$$E_{2x} = E_1 - \hbar^2 k_{II}^2 / 2m_2,$$

m_1 and m_2 are electron effective mass in GaAs and AlGaAs layers, respectively, U_0 is the barrier height, F is electric field strength in the barrier, d is the barrier width, E_1 is the kinetic energy of the incident carrier, and $k_{//}$ is the carrier wave vector component, parallel to the heterointerface.

The tunnelling probability across a triangular barrier is given by

$$D = \frac{4n}{p[Ai(h) + nBi'(h)]^2 + [Bi(h) - nAi'(h)]^2}, \qquad (2)$$

where

$$n = \frac{m_1 k_F}{m_2 k_{1x}},$$

$$k_F = (2m_2 eF/\hbar^2)^{1/3},$$

$$h = k_F(U_0 - E_{2x})/eF.$$

The other quantities in Eq.(2) have the same notations as in Eq.(1).

The details of the Monte Carlo simulation are described in [6,10,13,14]. The Poisson equation is solved on a spatial mesh with 2000 nodes. The potential distribution is updated at each time step Δt = 1 fs. The short time step was chosen in order to avoid the numerical instabilities associated with high carrier concentration. A spatial mesh with a large number of nodes was employed in order to evaluate precisely the shape of the potential distribution at the heterointerfaces, which shape is necessary for the accurate estimation of the tunnelling probabilities of each particle impinging the barrier. Results were obtained with 20,000 simulated particles. Calculations carried out with different numbers of particles showed that 20,000 simulated particles is sufficient for the achievement of high accuracy results.

The impact ionisation initiated by the electrons and holes was considered in the simulations, taking into account the secondary carriers created by impact ionisation [15]. The final states of the carriers after each ionisation event were determined as random quantities in such a way as to satisfy both energy and momentum conservation. The conventional probability distribution of the incident carrier states before and after ionisation, $S(\mathbf{k},\mathbf{k}') \propto (\mathbf{k}-\mathbf{k}')^{-4}$ was considered. The procedure is developed in such a way that the possible final states of the carriers cover completely the allowable momentum space for each individual ionisation event. The Keldysh formula $P = P_0 (E - E_t)^2 / E_t^2$ was accepted for the dependence of the ionisation probability against the energy E of the incident carrier. The values of the ionisation threshold energy E_t for electrons and holes were evaluated from energy and momentum conservation. The values of the adjustable coefficient P_0 for electrons and holes are estimated by ensuring the best agreement of the calculated ionisation coefficients in bulk material with the experimental data [16]. The impact ionisation in AlAs was disregarded in the calculations because the experimental results [16] demonstrated ionisation coefficients rapidly decreasing with the increase in the mole fraction x of $Al_xGa_{1-x}As$.

The *I-V* characteristic of the diode was calculated taking into account an external circuit. The series connected load resistance R_a = 50 Ω was accounted for self-consistently with the Monte Carlo simulations of the diode. The calculations were carried out for the device area S = 5000 μm^2. The behaviour of the circuit was governed by the equation

$$R_a C_0 \frac{dU_d}{dt} + U_d = U - R_a I_d, \qquad (3)$$

where C_0 is the geometric capacitance of the diode, U_d is the diode bias voltage, U is the bias voltage applied to the circuit, and I_d is the diode conduction current. This equation

was numerically solved simultaneously with the Monte Carlo particle simulations of the diode.

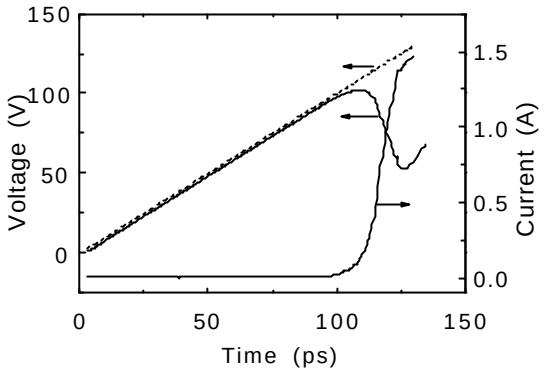

Fig. 2. The response of diode current and diode voltage (solid curves) to a ramp of circuit bias voltage raised linearly from U(0) = 0 to U(t) = 150 V (dashes) during t = 150 ps.

The calculated circuit response to the ramp of the circuit bias voltage *U(t)* is reported in Fig. 2. The results presented in Fig. 2 were obtained for *U(t)* linearly raised with time from $U = 0$ up to $U = 150$ V during 150 ps. As seen from Fig. 2, the diode is switched from the low conductance ("closed") state into the high conductance ("open") state when the diode bias voltage is close to $U_d = 100$ V. The *I-V* characteristic reported in Fig. 3 was obtained from the results presented in Fig. 2. The *I-V* characteristic exhibits a pronounced S-type dependence of the current upon bias voltage. The current-voltage instability associated with the S-type negative differential resistance R_d is damped by the external circuit because the condition $R_a^{-1} + R_d^{-1} < 0$ necessary for the development of the instability was not satisfied. The switching time is in the order of 10 ps as it is seen from the results presented in Fig. 2. The calculations carried out for the cross section area $S = 10000\ \mu m^2$ demonstrated essentially the same behaviour of the *I-V* characteristic. The switching time is raised to approximately 15 ps in a diode with the area $S = 10000\ \mu m^2$.

The analysis of the calculated results shows that the scenario of diode switching from the closed state to the open state is as follows: The calculated potential distributions corresponding to the closed and open states are reported in Fig. 4. In the closed state, the majority of the electrons are confined in the highly doped GaAs layers adjacent to the AlAs barriers.

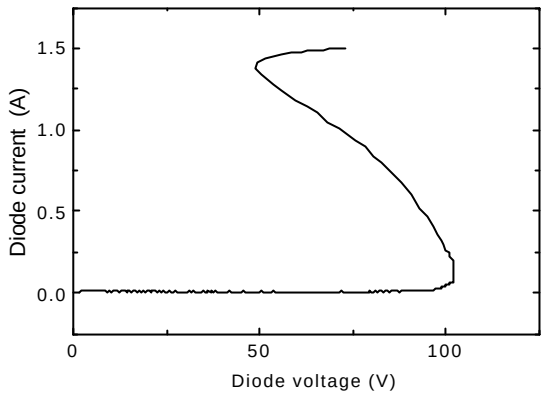

Fig. 3. Calculated current - voltage characteristic of the diode.

The electrons occupy the lowest Γ valley because the electric field in the doped GaAs regions is weak. Electron tunnelling from the doped GaAs layers into the AlAs barriers is responsible for current flow in the closed state. The electron energy is insufficient for the carriers to surmount the heterojunction barriers by thermionic emission due to the large band offset (1.03 eV). Intense impact ionisation does not develop in the low conductance state. Although the electric field is sufficiently high for interband impact ionisation in the undoped GaAs layers just before switching, the intense carrier multiplication does not originate because this region is depleted of electrons. As the bias voltage is further increased, the electric field in the AlAs layers is raised, and the potential barrier at the heterointerface becomes thinner and more permeable for electron tunnelling. Enhanced tunnelling current leads to the increase of the electron concentration in the AlAs barriers. These electrons, after crossing the AlAs barriers, enter the undoped GaAs layers, where the electric field is very high. As a result, the avalanche carrier multiplication develops due to intense impact ionisation in the undoped GaAs layers. The intensity of electron impact ionisation is additionally enhanced by the conduction band offset between AlAs and GaAs [17,18]. Furthermore, the electrons and holes generated by the ionisation are partially confined by the conduction and valence band offsets at the GaAs/AlAs interfaces. This leads to an additional increase of the electric field at the interfaces, and, consequently, the

tunnelling current grows as a consequence. As a result, the diode is switched to the open state. The potential is redistributed in the open state as shown in Fig. 4. In this state, the high electric field in the AlAs barriers and the enhancement of the carrier energy by the band offset between AlAs and GaAs is still sufficient for maintaining impact ionisation in the open state.

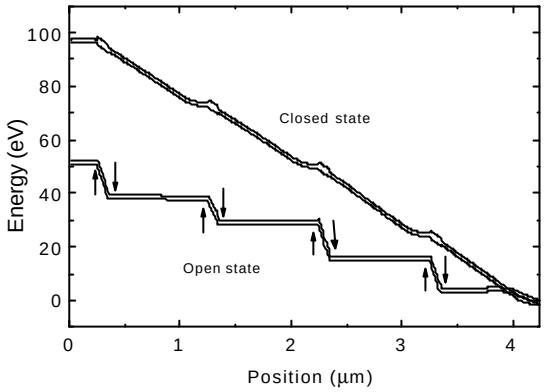

Fig. 4. Potential (the edge of Γ valley and the top of heavy hole subband) distributions in the low and high conductance states. The results were obtained under the same conditions as in Fig. 3 and correspond to the time moments t = 90 ps for the low conductance state, and to t = 130 ps for the high conductance state, respectively. The upper and lower arrows indicate the regions in which an intensive impact ionisation is initiated by electrons and holes, respectively, in the open state.

The stability of the diode, both in the closed and open states, was investigated by Monte Carlo simulations under the conditions of a constant bias voltage applied to the circuit. The results of the calculations show that the diode is not switched to the high conductance state at least during 300 ps when the circuit bias voltage is just below the switching voltage U = 90 V. Also, the diode is sustained in the open state for at least during 300 ps when the constant bias voltage U=130 V is applied to the circuit. No evidence of diode switching from the one state to the another was observed from Monte Carlo simulations during 300 ps.

Because the switching process is initiated by the avalanche carrier multiplication in the undoped GaAs layers, the value of the switching voltage is determined by the length and number of unit cells. The condition for the onset of the avalanche multiplication initiated by electrons is given by $M > 1$, where [19]

$$M = \int_0^L a(x) \exp\left\{-\int_0^x [a(x') - b(x')]dx'\right\} dx \qquad (4)$$

Here a and b are electron and hole ionisation coefficients, respectively, and L is the length of the region in which the impact ionisation takes place. The electric field strength F in undoped GaAs layers is nearly uniform just after switching. According to the results of the calculations, F is close to 300 kV/cm in the undoped GaAs layers when the diode bias voltage corresponds to the switching voltage. The values of the ionisation coefficients in GaAs at F = 300 kV/cm are [16]: $\alpha = 7300\ \text{cm}^{-1}$ and $\beta = 4300\ \text{cm}^{-1}$. The total length of the undoped GaAs layers in the device is L = 2.6 μm. By substituting the numerical values of α, β and L into Eq. (4) we obtain M = 1.3, thus the condition for the development of the avalanche multiplication is satisfied.

We note that the switching voltage is proportional to the number of unit cells. Simulations of two-barrier and three-barrier diodes demonstrated switching voltages of 50 V and 75 V, respectively. It can be expected that a further increase in the number of unit cells above the four used in this simulation will result in the increase of the switching voltage to above 100 V. Also, one can anticipate that the switching time will not rise due to internal current amplification which is conditioned by carrier multiplication induced by impact ionisation. The switching time is determined by the rate of space charge redistribution inside the unit cells. Because the potential barriers of the heterojunctions are sufficiently high, most of the created carriers are confined at the heterointerfaces. Therefore, the switching time can be estimated roughly as the time duration of carrier drift across the GaAs layer of the unit cell. By assuming electron and hole drift velocity to be 10^7 cm/s, we obtain a switching time of 9 ps which is in close agreement with the Monte Carlo results.

The simulation of the circuit response to a circuit bias voltage which is decreasing from U = 200 V to U = 0 V during a period of 200 ps showed that the closing time of the device is on the same order as the opening time. According to the results of simulation the intensity of impact ionisation in the GaAs layers at the heterointerfaces becomes insufficient to maintain the staircase shape of the potential distribution (Fig. 4, open state) when the diode bias voltage is reduced to a value below 50 V. The electrons and holes confined at heterointerfaces are extracted due to tunnelling and thermoemission processes. As a result, the potential distribution becomes linear, and the device is switched to the closed state.

In conclusion, a new multibarrier heterostructure switch is proposed. It was investigated by Monte Carlo particle simulations. The switching phenomenon is based

on electron tunnelling and thermoemission from the GaAs wells to the AlAs barriers, electron drift across the AlAs barriers, followed by subsequent impact ionisation in the undoped GaAs layers. The calculated switching voltage is close to 100 V for a diode involving four AlAs barriers at 300 K lattice temperature. The estimated switching time is in the order of 10 ps.

This work was supported by the US Ballistic Missile Defence Organisation, by the US Air Force's European Office of Aerospace R&D under contract F61775-98-WE011 and by Lithuanian Science Foundation.

REFERENCES

1. K. Hess, T. K. Higman, M. A. Emanuel, J. J. Coleman, *J. Appl. Phys*. **60**, p.3775 (1986).

2. J. N. Baillargeon, K. Y. Cheng, J. Laskar, J. Kolodzey, *Appl. Phys. Lett.* **55**, p.663 (1989).

3. C. Song, K. P. Roenker, *J. Appl. Phys.* **72**, p.4417 (1992).

4. W. C. Hsu, W. C. Liu, D. F. Guo, W. S. Lour, *Appl. Phys. Lett.* **62**, p.1504 (1993).

5. W. C. Liu, D. F. Guo, S. R. Yih, J. T. Liang, L. W. Liah, *Appl. Phys. Lett.* **64**, p.2685 (1994).

6. A. Reklaitis, R. Stasch, M. Asche, A. Krotkus, E. Schoell, *J. Appl. Phys*. **82**, p.1706 (1997).

7. D. F. Guo, *Appl. Phys. Lett*. **71**, p.1219 (1997).

8. A.Reklaitis, *Abstracts of 20th Workshop on Compound Semiconductor Devices and Integrated Circuits*, Vilnius 1996, p.95.

9. A. Reklaitis, *J.Appl. Phys*. (in press).

10. A. Reklaitis, *J. Appl. Phys*. **80**, p.1242 (1996).

11. S. Adachi, *J. Appl. Phys*. **58**, R1 (1985).

12. C. N. Yeh, L. E. McNeil, L. J. Blue, T. D. Race, *J. Appl. Phys*. **77**, p.4541 (1995).

13. A. Reklaitis, *Proc. Third ELEN Workshop* (edited by C. Clayes and E.Simoen, Leuven, Belgium, 1996), p.108.

14. A. Reklaitis, L. Reggiani, *J. Appl. Phys*. **82**, p.3161 (1997).

15. A. Reklaitis, *J. Phys. Chem. Solids* **42**, p.891 (1981).

16. V. M. Robbins, S. C. Smith, G. E. Stillman, *Appl. Phys. Lett*. **52**, p.296 (1988).

17. R. Chin, N. Holonyak, G. E. Stilman, J. Y. Tang, K. Hess, *Electron. Lett*. **16**, p.468 (1980).

18. F. Capasso, W. T. Tang, A. L. Hutchison, G. F. Williams, *Appl. Phys. Lett*. **40**, p.38 (1982).

19. S. M. Sze, *Physics of Semiconductor Devices* (Wiley , New York, 1981).